A Journal of the Gesellschaft Deutscher Chemiker

Angewandte International Edition

GDCh

Chemie

www.angewandte.org

Accepted Article

Title: Template- and Metal-free Synthesis of Nitrogen-rich Nanoporous Noble Carbon Materials by Direct Pyrolysis of a Preorganized Hexaazatriphenylene Precursor

Authors: Ralf Walczak, Bogdan Kurpil, Aleksandr Savateev, Tobias Heil, Johannes Schmidt, Qing Qin, Markus Antonietti, and Martin Oschatz

To be cited as: *Angew. Chem. Int. Ed.* 10.1002/anie.201804359
Angew. Chem. 10.1002/ange.201804359

Link to VoR: http://dx.doi.org/10.1002/anie.201804359
http://dx.doi.org/10.1002/ange.201804359

WILEY-VCH

10.1002/anie.201804359

WILEY-VCH

Template- and Metal-free Synthesis of Nitrogen-rich Nanoporous Noble Carbon Materials by Direct Pyrolysis of a Preorganized Hexaazatriphenylene Precursor

Ralf Walczak,[a] Bogdan Kurpil,[a] Aleksandr Savateev,[a] Tobias Heil,[a] Johannes Schmidt,[b] Qing Qin,[a] Markus Antonietti,[a] and Martin Oschatz*[a]

Abstract: The targeted thermal condensation of porous and oxidation resistant ("noble") carbons starting from a hexaazatriphenylene precursor is reported. Simple condensation of the pre-aligned molecular precursor leads to nitrogen-rich carbons with C_2N-type stoichiometry. Despite the absence of any porogen and metal species involved in the syntthesis, specific surface areas reach of the molecular carbons up to 1000 $m^2 g^{-1}$ due to the significant microporosity of the materials. The content and type of nitrogen species is controllable by the carbonization temperature whilst porosity remains largely unaffected at the same time. The resulting noble carbons stand out by a highly polarizable micropore structure and have thus high adsorption affinity towards molecules such as H_2O and CO_2. This molecular precursor approach opens new possibilities for the synthesis of porous noble carbons under molecular control accessing the special physical properties of the C_2N structure, extending the known spectrum of classical porous carbons.

Sp^2-based carbon nanomaterials[1] combine many attractive properties such as high electrical conductivity and abundant availability. In consequence, these materials are widely applied in crucial fields of energy and environment, like adsorption processes,[2] catalysis,[3] and energy storage and conversion.[4] Carbons have the smallest voxel size for chemical construction, and their properties can be adjusted over a wide range by tailoring their atomic framework construction. Substitution of graphene 6-rings by other structure motives like 5-rings, 7-rings or defect sites leads to structure distortion, and if the arrangement becomes completely random it will finally result in a high surface area porous framework.

Besides geometrical structure engineering, carbon-based materials can also be widely tailored in terms of their electronic and surface atomic structure by heteroatom-doping.[5] Incorporation of nitrogen into the carbon framework is widely studied and leads to N-doped carbons (NdCs) or carbon nitrides (CNs) with different stoichiometry. Such materials are much more "noble" than pristine carbon, that is, they oxidize matter rather than being oxidized due to the very positive working potential of their electrons.[6] NdCs and CNs are widely applied as stabilizers for metal catalysts[7] or in energy storage applications[8] and typically provide beneficial properties as compared to non-noble carbon materials obtained by established processes such as carbonization of sugar.

In addition to their higher oxidation resistance, NdCs and CNs have significant advantages over traditional carbons in the field of adsorption from gas and liquid phase. The heteroatom-doping makes the conjugated structure much stronger polarizing and can provide specific binding sites, both leading to significantly higher enthalpies of interaction between the adsorbent and the guest species, when compared to ordinary activated carbons. For instance, enhanced interaction has been observed in CO_2[9] and H_2O[10] gas adsorption, adsorption of ions from solution[8b, 8e] or ionic liquid ions[8c] for carbons with substantial nitrogen content. In all those cases, heteroatom doping leads to strong binding of the respective guest species. This is the fundamental reason why noble carbons are even able to catalyze chemical conversions without addition of metals, as it is typical for established catalytic processes.[11]

In most cases, these significant advantages of NdCs and CNs over pristine carbon materials can only be accomplished if (i) the heteroatom-containing structure motives are well defined, large in number, and tailorable in chemical composition; (ii) the material provides a large surface area to allow for sufficient access to the entire atomic framework (or in other words to maximize the synergistic effect between surface heterogeneity and surface area); and (iii) the materials are clean of any unwanted impurities such as metal atoms or metal ions.

From a synthetic perspective it seems to be attractive to synthesize such NdC or CN materials from precursors where the nitrogen atoms are already suitably preorganized.[12] In such molecules, the nanoarchitecture of the heteroatom-containing structure motives already exists and their controlled carbonization leads to more regular condensation towards N-rich noble carbons. This principle is already widely applied to address the above-mentioned point (i) but the introduction of porosity and thus large available surface area in such materials remains template-based and thereby indirect. Here we report a template-free synthesis of highly microporous noble carbon materials with large and controllable nitrogen content and a stoichiometry close to C_2N by direct carbonization of the hexaazatriphenylene (HAT) precursor (Supporting Information, Figure S1a).[13] HAT is an electron deficient, rigid, planar, aromatic discotic system with an excellent π–π stacking ability and remarkable oxidation resistance (Figure S1b).[14] Especially its strong supramolecular aggregation and the ability to self-assemble into crystalline structures (Figures S1c and S1d) make it a promising material for the synthesis of noble carbons. To our knowledge, direct carbonization of HAT derivatives towards noble carbons has not been reported so far.

A series of porous CN materials was synthesized *via* condensation of hexaazatriphenylene-hexacarbonitrile (HAT-

[a] R. Walczak, Dr. B. Kurpil, Dr. A. Savateev, Dr. T. Heil, Q. Qin, Prof. M. Antonietti, Dr. M. Oschatz
Kolloidchemie
Max Planck Institut für Kolloid- und Grenzflächenforschung
Am Mühlenberg 1, 14476 Potsdam, Germany
E-mail: martin.oschatz@mpikg.mpg.de

b] Dr. J. Schmidt
Institut für Chemie Chemistry, Abteilung Funktionsmaterialien
Technische Universität Berlin
Hardenbergstraße 40, 10623 Berlin, Germany

Supporting information for this article is given via a link at the end of the document.

CN) under nitrogen flow (Figures S1a and S1b). The nitrogen-rich ($C_{18}N_{12}$) organic molecule was heated to 550, 700, 850, or 1000 °C without any pretreatment, and the resulting carbonized C-HAT-CN-X materials are labelled according to their carbonization temperature. Nanoporous carbon nitrides can hence be obtained without the use of any template during synthesis, and no additional washing step after carbonization is necessary due to the absence of residual inorganic porogens. Because already the HAT precursor is fully sp^2-hybridized and free of hydrogen, further condensation can take place without the need for elimination or oxidation and thus is solely based on π-electrocyclic rearrangements as proposed in Figure 1. Indeed, the investigation of the HAT condensation mechanism by thermal analysis (under helium flow) coupled with mass spectrometry (TGA-MS) reveals that the main elimination products are CN-type species resulting from the splitting-off of nitrile groups of HAT monomers (Figure S2).

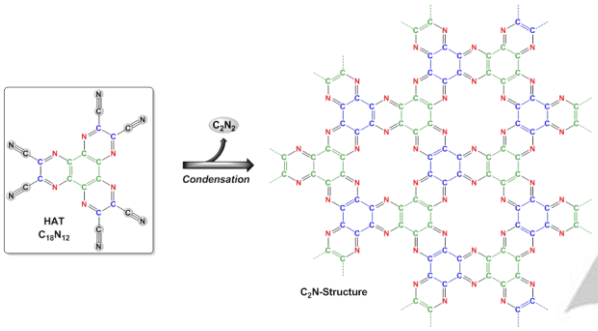

Figure 1: Idealized model for the formation of a C_2N structure by condensation of HAT-CN precursor.

The as-synthesized materials show comparable microscale morphology to the primary HAT-CN crystals, that is, they appear as an accumulation of small flat plates exhibiting a smooth surface (Figure S3a–d). Thus, the macrostructure induced by the pre-organization of HAT-CN can be transferred to the carbonized products. At higher temperature, condensation causes fracturing and several gaps (~100–200 nm in size) open evenly over the surface of the pallets. The fracturing of the flat plates reveals their set-up from small primary spheres which are randomly packed.

The results of the C/H/N elemental analysis (EA), energy-dispersive X-ray (EDX) spectroscopy, and the elemental compositions obtained by X-ray photoelectron spectroscopy (XPS) analysis show that lower synthesis temperatures results in higher nitrogen content in the C-HAT-CN-X materials (Table 1). Nitrogen contents of 29.4 at.% (EA) and 32.7 at.% (XPS) suggest a nearly perfect C_2N-type stoichiometry in C-HAT-CN-550, as previously reported by *Fechler et al*.[15] and *Mahmood et al.*.[16] Thus, the stoichiometric composition predictated by HAT-CN can be transferred to the C_2N products due to the controlled condensation mechanism. The homogeneous distribution of carbon and nitrogen is shown in the EDX mapping patterns independent of the synthesis temperature (Figure 2a–d). The uniform porous nanostructure after HAT-CN condensation can be observed in high-resolution transmission electron microscopy (HRTEM; Figure 2e–h) images of C-HAT-CN-550 and C-HAT-CN-700. For C-HAT-CN-850 and C-HAT-CN-1000, structures are characterized by concentric spherical graphitic shells, which are interpenetrated and overlapping, thus revealing a structural rearrangement after carbonization at higher temperatures due to transition from a noble carbon to a rather graphitic carbon phase poor of heteroatoms.

X-ray photoelectron spectra (XPS; Figure S4a–d) were recorded to identify the different bonding characteristics of nitrogen and carbon atoms in these materials. Deconvolution of the N1s line scans (Figure 3a–d; Tables S1 and S2) reveals the presence of cyano- and pyrazine groups, corresponding to the signals at binding energies of ~398 eV and ~399 eV. The peaks at ~400–401 eV and ~402–403 eV correspond to quaternary nitrogen atoms and oxidized nitrogen, respectively. The ratio between nitrogen atoms from cyano and pyrazine groups and quaternary nitrogen atoms can be controlled by the synthesis temperature since the decrease of nitrogen content at higher temperatures is mainly on the expense of cyano and pyrazine groups as present in HAT-CN (Tables S1 and S2). The amount of quaternary nitrogen with higher binding energy and thus also higher nobility in the total carbon nitride material increases at medium carbonization temperatures and decreases again at 1000 °C. In contrast, the cyano and pyrazinic nitrogen content of the noble carbons decreases continuously from 550 °C (25.5 at.%) to 1000 °C (1.8 at.%). Deconvolution of the C1s spectra (Figure S5a–d; Tables S1 and S2) reveals a peak at ~284 eV that belongs to graphitic C=C carbons, while two peaks at ~285 eV and ~286 eV correspond to carbons bonded to sp^2-hybridized nitrogen atoms. Oxidized carbon atoms can be assigned to the peak at ~289–290 eV. All single peaks as well as the full line scan are shifted to lower binding energy with increasing synthesis temperature, indicating a decrease of the noble character and less positive working potential of the electrons, i.e. the nobility is lost again when heating to too high temperatures.

Table 1: EA, EDX, XPS, Argon physisorption (87 K), and Raman spectroscopy data summary as well as experimental carbon yield of the C-HAT-CN-X materials.

Temp.	**C** / at.%			**N** / at.%			**O** / at.%			SSA_{BET} / $m^2\ g^{-1}$	SSA_{QSDFT} / $m^2\ g^{-1}$	V_{CO2} (<1.5 nm) / $cm^3\ g^{-1}$	V_{Ar} (<2 nm) / $cm^3\ g^{-1}$	I_D/I_G	Yield / %
	EA	EDX	XPS	EA	EDX	XPS	EA	EDX	XPS						
550	48.3	58.9	64.0	29.4	39.7	32.7	-	1.4	3.3	627	1013	0.28	0.24	0.58	50
700	47.7	61.2	67.0	24.3	37.1	29.8	-	1.7	3.2	785	1182	0.33	0.30	0.91	33
850	51.3	62.4	69.9	20.0	35.9	24.6	-	1.7	4.7	814	1137	0.30	0.31	1.37	27
1000	67.8	96.5	90.1	4.9	-	7.4	-	3.5	2.6	801	1148	0.32	0.31	1.80	25

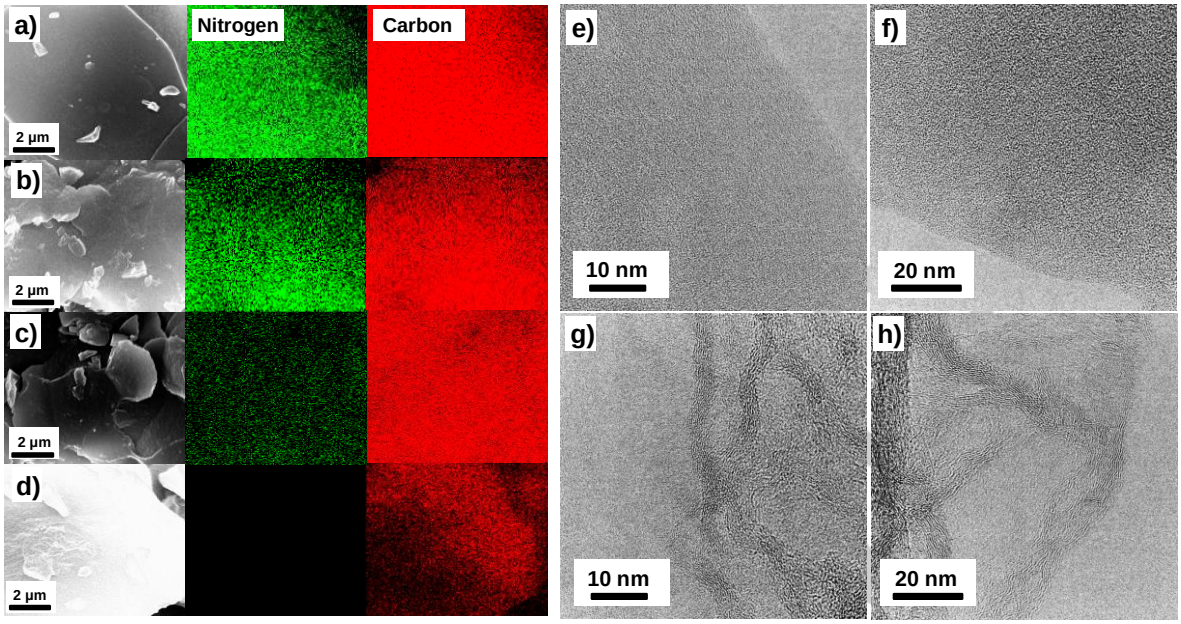

Figure 2. SEM images with elemental mapping (a–d) of N (green), and C (red), as well as HRTEM images (e–h) of C-HAT-CN-550 (a and e), C-HAT-CN-700 (b and f), C-HAT-CN-850 (c and g), and C-HAT-CN-1000 (d and h).

The on-going development of a nitrogen-free graphitic carbon phase at higher synthesis temperature can be seen by the growing contribution of C=C bonds. In accordance to the results of the N1s spectra, the peak corresponding to sp^2-nitrogen peak significantly decreases at higher carbonization temperature. All in all, the XPS measurements underline the comparably precise control over the atomic structure and the high nitrogen content that can be achieved in such CN materials made of HAT-CN.

Powder X-ray diffraction measurements (Figure S6) confirm the absence of crystalline inorganic impurities and indicate an amorphous structure as it is typical for high surface area carbons such as the C-HAT-CN-X materials due to the absence of sharp peaks that correspond to graphitic stacking. However, the increasing intensity of the peak between 25 and 30 ° 2θ suggests the reoccurance of graphitic stacking at higher carbonization temperatures in agreement with HRTEM investigations.

Raman spectroscopy (Figures S7 and S8a–d) is another useful tool to characterize sp^2-based carbon structures by their so-called disordered (D) and graphite (G)-like bands with varying intensity, position, and width. It should be noted that the standard interpretation of Raman spectra as applied for pristine carbons cannot be strictly applied to nitrogen-containing carbons (as nitrogen-doping is a source of vibrational dissymmetry), but some interesting information on the progress of carbonization can still be derived. The spectra have been fitted with a three-band model including the D-band (breathing mode of sp^2-carbon atoms in aromatic rings), G-band (sp^2-carbon organized in chains or rings), and the D^2-band (assigned to *trans*-polyacetylene-like chains at layer edges). In our series of samples, the I_D/I_G ratio increases constantly from 0.58 to 1.80 with increasing synthesis temperature (Table 1) due to the favored organization of sp^2-bonded carbon atoms in six-rings and a smaller amount of substitutional N atoms, that is, the ongoing formation of a phase of pristine carbon. This, in turn, will lead to a higher electrical conductivity of the samples prepared at higher temperatures. A higher carbon symmetry for the samples synthesized at higher temperatures is also suggested by the decreased intensity of the shoulder D^2-band.

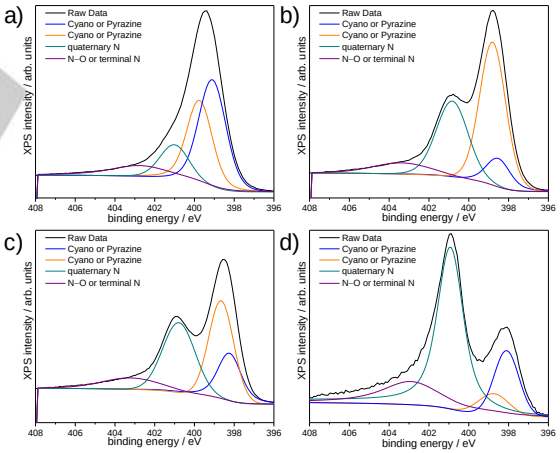

Figure 3. Fitted N1s XPS line scans of C-HAT-CN-550 (a), C-HAT-CN-700 (b), C-HAT-CN-850 (c), and C-HAT-CN-1000 (d).

TGA under air (Figure S9) show that C-HAT-CN-550 – the most noble compound with the highest nitrogen content – reveals the highest onset of the decomposition temperature in air of ~500 °C. The increase in onset temperature for the materials prepared at lower temperatures can be explained by the near-perfect C_2N stoichiometry and absence of a free carbon phase. Thus, C-HAT-CN-550 has the highest oxidation resistance. TGA-MS measurements (Figures S10a and S10b) show that this sample shows a typical feature of noble carbons, which is its thermal

decomposition into stable monomers rather than oxidation. Carbon-nitrogen compounds such as HCN, N_2, N_2H_2 are the main products of sublimation, whereas CO_2 is only a minor reaction product. In contrast, C-HAT-CN-1000 has a large contribution of free carbon and is thus combusted to CO_2 while the remaining nitrogen is released as HCN. The high stability of the HAT-CN precursor leads to a thermal stability of the noble carbon structure which cannot be achieved by utilization of classical carbon precursors such as sugars or biomaterials.

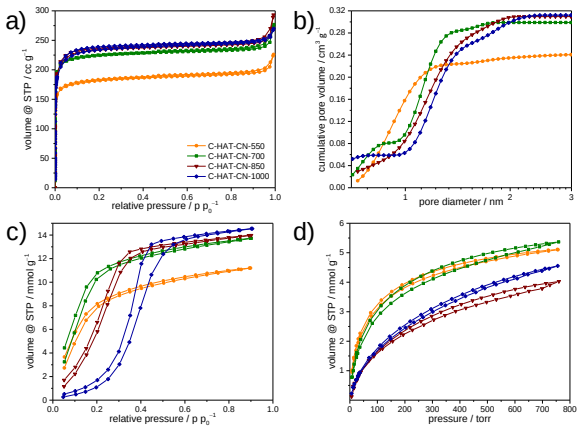

Figure 4. Argon physisorption isotherms (87 K) (a), corresponding cumulative pore size distribution plot calculated with QSDFT (Argon on carbons with cylindrical/sphere pores at 87 K, adsorption branch kernel) (b), water vapour physisorption isotherms at 298 K (c), and carbon dioxide physisorption isotherms at 273 K (d) of C-HAT-CN-550 (orange circles), C-HAT-CN-700 (green squares), C-HAT-CN-850 (wine triangles), and C-HAT-CN-1000 (blue diamonds).

Argon physisorption isotherms of the C-HAT-CN-X materials recorded at 87 K (Figure 4a and Figure S11) are type Ia isotherms according to the IUPAC classification[17] with a large uptake of gas at low relative pressure and no further adsorption at $p\,p_0^{-1}$ = 0.1–0.9 and thus reveal the practically exclusive microporous character of the HAT-derived carbons. In spite of the absence of any inorganic porogen, these materials provide high specific (multi-point) BET ($0.005 < p/p_0 < 0.05$) surface areas (SSA_{BET}; Figure S12) in the range of 600–800 $m^2\,g^{-1}$. SSAs determined by the quenched solid density functional theory (QSDFT) method (Figure S13) are even slightly higher (Table 1). Solely the condensation of the initially non-porous HAT crystals (SSA_{BET} ~4 $m^2\,g^{-1}$) is responsible for the development of significant microporosity, which can be regarded as “structural”, i.e. typical for the geometry and angularity of the polycondensed framework, see also the structure of C_2N. With increasing condensation temperature, micropores are enlarged and this is leading to the increase of micropore volume (Figure 4b and Figure S14, Table 1). In particular, a large volume of accessible microporosity is created by condensation in the 550–700°C regime due to more well-defined arrangement and stacking in the C-HAT-CN-700 as supported by the rather open microstructure in HRTEM images (Figure S15). The Ar uptake at $p\,p_0^{-1} > 0.9$ is likely due to adsorption on the external surface of the small bullets within the flakes providing a certain hierarchy into the pore system of the C-HAT-CN-X materials as well.

Due to their strongly polarizing surface structure in combination with narrow microporosity, the porous C_2N materials show very high H_2O adsorption capability even at relative pressures below $p\,p_0^{-1}$ = 0.2 (6000 ppm). All isotherms are of type I (Figure 4c). Considering the accessible pore volume of 0.35 $cm^3\,g^{-1}$ (calculated by addition of the CO_2 pore volume below 1.5 nm and the Argon pore volume above 1.5 nm), the uptake (10.22 mmol g^{-1}) of C-HAT-CN-700 translates to a density of 17–18 water molecules per nm^3. In other words, the density of water would be more than 0.5 $cm^3\,g^{-1}$ at a concentration of only 6000 ppm. To our knowledge, comparable strong affinity of carbonaceous structures to water molecules is so far only reported for a few highly nitrogen doped materials produced by rather sophisticated methods using metal salts, solvents, and more systhesis steps.[10, 18] The packing density in our HAT-derived samples is, however, still about 50% higher which is likely caused by their significantly higher nitrogen content at lower oxygen contribution and even more narrow micropores. The adsorption capacity of C-HAT-CN-550 is a bit lower at $p\,p_0^{-1}$ = 0.2, which presumably is caused by its lower microporosity and thus lower adsorption capacity in spite of its even higher affinity towards water due to the higher nitrogen content. With the increase of the condensation temperature the onset points of water adsorption shift to higher relative pressures and the presence of a hysteresis in case of the nitrogen-poor C-HAT-CN-1000 shows the transition of the water adsorption mechanism to the one that is typical for microporous carbon materials with less polar sites. The comparable uptake of the materials produced at 700, 850, and 1000 °C and the slightly lower saturation volume of C-HAT-CN-550 are well in line with the pore volume trends observed in Ar physisorption experiments.

The strong polarization of gas molecules by the C-HAT-CN-X materials is also obvious in CO_2 adsorption experiments at 273 K (Figure 4d). Due to their higher nitrogen content, C-HAT-CN-550 and C-HAT-CN-700 show a CO_2 physisorption isotherm with a rather convex shape due to a high affinity to CO_2 at low pressure and thus very strong adsorption. Their uptake at 1 bar (5.09 mmol g^{-1} for C-HAT-CN-550, 5.34 mmol g^{-1} for C-HAT-CN-700) may not appear outstanding as such but in view of the low total pore volume, the volume of adsorbed CO_2 is very high. For microporous carbons without significant heteroatom content, the pore volume to achieve such high uptake must be around twice as high – even when the pore size is optimized for CO_2 adsorption.[19] Accordingly, thermal response measurements with the InfraSORP technique of CO_2 adsorption on the HAT-derived carbons at 298 K and 1 bar (Figure S16) show mass- and pore volume-related thermal response peak areas between 22 and 41 $mg^{-1}\,cm^{-3}$. This is significantly higher than for microporous carbon materials with comparable pore size but without heteroatom functionalization.[20] This further indicates the very strong affinity and high binding enthalpy of HAT-CN-derived carbons to CO_2.

C-HAT-CN-550 shows a CO_2 uptake of 3.24 mmol g^{-1} at 273 K and p = 0.15 bar. This value is in the range of the leading materials for CO_2 capture which often have far higher micropore volumes.[21] Initially one could now assume that these HAT-

derived carbons are attractive materials for CO_2 capture at low concentrations, e.g., for filtration of the molecule from flue gases. At 298 K and a N_2/CO_2 ratio of 90/10, which are benchmark conditions for this application, the selectivity of C-HAT-CN-550 and C-HAT-CN-700 is 63.8 and 53.6, respectively (Figure S17). These values are not exceedingly high, and the likely reason for this is that the pores are still large enough to host significant amounts of N_2. Due to its significant quadrupole moment it will be attracted by the strong polarization inside the C-HAT-CN-X materials in a comparable way as CO_2 as we have pointed out in a recent review article.[21] In other words, these materials are not really attractive for CO_2 selective capture – especially if the similar high affinity to H_2O is taken into consideration, which will lead to less selective CO_2 capture under real world conditions. The strong CO_2 binding is more attractive for the activation of the molecule with regard to its catalytic conversion rather than its selective capture in the presence of other gases. Preliminary tests of the C-HAT-CN-700 in electrocatalytic CO_2 reduction (Figure S18) show that there is a significant current enhancement in CO_2-saturated solution in comparison to N_2-saturated solution indicating the high catalytic activity.

In conclusion, we have reported a novel template-free synthesis pathway towards microporous noble carbon materials with nearly perfect C_2N-type stoichiometry and high purity by controlled condensation of preorganized HAT precursor molecules. The significant amount of heteroatoms in these materials leads to outstanding adsorption properties, as indicated by high uptake of guest molecules such as H_2O and CO_2 at low concentrations resulting from the combination of strong polarization on specific adsorption sites and high micropore volume. The C_2N-type material is thus a promising metal-free alternative for various catalytic conversions. The precise atomic-level structural control over the carbon microstructure provided by the controlled condensation of precursor molecules like HAT-CN enables the controlled synthesis of carbon materials with stabilities even exceeding those of established porous carbons and with adsorption properties which are so far only achieved with metal-organic frameworks or zeolites.

Experimental

Details of synthetic procedures and characterization methods can be found in the supporting information of this article.

Acknowledgements

M.O. and R.W. acknowledge financial support by a Liebig Scholarship of the German Chemical Industry Fund (Stiftung Stipendien Fonds der Chemischen Industrie, FCI).

Keywords: carbon materials • hexaazatriphenylene • porosity • nitrogen doping • physisorption

[1] *Carbon Nanomaterials* (Eds.: Y. Gogotsi, V. Presser), CRC Press, Boca Raton, **2014**.

[2] a) M. Oschatz, L. Borchardt, M. Thommes, K. A. Cychosz, I. Senkovska, N. Klein, R. Frind, M. Leistner, V. Presser, Y. Gogotsi, S. Kaskel, *Angew. Chem.* **2012**, *124*, 7695; *Angew. Chem. Int. Ed.* **2012**, *51*, 7577; b) R. E. Morris, P. S. Wheatley, *Angew. Chem.* **2008**, *120*, 5044; *Angew. Chem. Int. Ed.* **2008**, *47*, 4966.

[3] a) *Carbon Materials for Catalysis* (Eds.: P. Serp, J. L. Figueiredo), John Wiley & Sons, Hoboken, **2009**; b) D. S. Su, S. Perathoner, G. Centi, *Chem. Rev.* **2013**, *113*, 5782.

[4] a) L. Borchardt, M. Oschatz, S. Kaskel, *Mater. Horiz.* **2014**, *1*, 157; b) L. Dai, D. W. Chang, J. B. Baek, W. Lu, *Small* **2012**, *8*, 1130; c L. Borchardt, M. Oschatz, S. Kaskel, *Chem.-Eur. J.* **2016**, *22*, 7324; d) M. S. Mauter, M. Elimelech, *Environ. Sci. Technol.* **2008**, *42*, 5843; e) R. Y. Yan, T. Heil, V. Presser, R. Walczak, M. Antonietti, M. Oschatz, *Adv. Sustainable Syst.* **2017**, 1700128.

[5] a) J. P. Paraknowitsch, A. Thomas, *Energy Environ. Sci.* **2013**, *6*, 2839; b) S. Zhang, S. Tsuzuki, K. Ueno, K. Dokko, M. Watanabe, *Angew. Chem.* **2015**, *127*, 1318; *Angew. Chem. Int. Ed.* **2015**, *54*, 1302.

[6] M. Antonietti, M. Oschatz, *Adv. Mater.* **2018**, *30*, 1706836.

[7] a) Y. Gong, M. Li, H. Li, Y. Wang, *Green Chem.* **2015**, *17*, 715; b) M. Oschatz, J. P. Hofmann, T. W. van Deelen, W. S. Lamme, N. A. Krans, E. J. Hensen, K. P. de Jong, *ChemCatChem* **2017**, *9*, 620; c) H. J. Schulte, B. Graf, W. Xia, M. Muhler, *ChemCatChem* **2012**, *4*, 350.

[8] a) Z. Wen, X. Wang, S. Mao, Z. Bo, H. Kim, S. Cui, G. Lu, X. Feng, J. Chen, *Adv. Mater.* **2012**, *24*, 5610; b) C. Schneidermann, N. Jäckel, S. Oswald, L. Giebeler, V. Presser, L. Borchardt, *ChemSusChem* **2017**, *10*, 2416; c) J. K. Ewert, D. Weingarth, C. Denner, M. Friedrich, M. Zeiger, A. Schreiber, N. Jäckel, V. Presser, R. Kempe, *J. Mater. Chem. A* **2015**, *3*, 18906; d) F. Pei, T. An, J. Zang, X. Zhao, X. Fang, M. Zheng, Q. Dong, N. Zheng, *Adv. Energy Mater.* **2016**, *6*, 1502539; e) J. Zhao, H. Lai, Z. Lyu, Y. Jiang, K. Xie, X. Wang, Q. Wu, L. Yang, Z. Jin, Y. Ma, J. Liu, Z. Hu, *Adv. Mater.* **2015**, *27*, 3541.

[9] a) X. Ren, H. Li, J. Chen, L. Wei, A. Modak, H. Yang, Q. Yang, *Carbon* **2017**, *114*, 473; b) M. Sevilla, P. Valle-Vigón, A. B. Fuertes, *Adv. Funct. Mater.* **2011**, *21*, 2781.

[10] G. P. Hao, G. Mondin, Z. Zheng, T. Biemelt, S. Klosz, R. Schubel, A. Eychmüller, S. Kaskel, *Angew. Chem.* **2015**, *127*, 1962; *Angew. Chem. Int. Ed.* **2015**, *54*, 1941.

[11] a) Y. Wang, X. Wang, M. Antonietti, *Angew. Chem.* **2012**, *124*, 70; *Angew. Chem. Int. Ed.* **2012**, *51*, 68-89; b) A. Thomas, A. Fischer, F. Goettmann, M. Antonietti, J.-O. Müller, R. Schlögl, J. M. Carlsson, *J. Mater. Chem.* **2008**, *18*, 4893; c) Y. Zheng, Y. Jiao, L. Ge, M. Jaroniec, S. Z. Qiao, *Angew. Chem.* **2013**, *125*, 3192; *Angew. Chem. Int. Ed.* **2013**, *52*, 3110.

[12] A. Savateev, S. Pronkin, J. D. Epping, M. G. Willinger, M. Antonietti, D. Dontsova, *J. Mater. Chem. A* **2017**, *5*, 8394.

[13] J. L. Segura, R. Juarez, M. Ramos, C. Seoane, *Chem. Soc. Rev.* **2015**, *44*, 6850.

[14] B. Kurpil, A. Savateev, V. Papaefthimiou, S. Zafeiratos, T. Heil, S. Özenler, D. Dontsova, M. Antonietti, *Appl. Catal. B: Environ.* **2017**, *217*, 622.

[15] N. Fechler, N. P. Zussblatt, R. Rothe, R. Schlogl, M. G. Willinger, B. F. Chmelka, M. Antonietti, *Adv. Mater.* **2016**, *28*, 1287.

[16] J. Mahmood, E. K. Lee, M. Jung, D. Shin, I. Y. Jeon, S. M. Jung, H. J. Choi, J. M. Seo, S. Y. Bae, S. D. Sohn, N. Park, J. H. Oh, H. J. Shin, J. B. Baek, *Nat. Commun.* **2015**, *6*, 6486.

[17] M. Thommes, K. Kaneko, A. V. Neimark, J. P. Olivier, F. Rodriguez-Reinoso, J. Rouquerol, K. S. W. Sing, *Pure Appl. Chem.* **2015**, *87,* 1051-1069.

[18] G.-P. Hao, C. Tang, E. Zhang, P. Zhai, J. Yin, W. Zhu, Q. Zhang, S. Kaskel, *Adv. Mater.* **2017**, *29*, 1702829.

[19] M. Oschatz, H. C. Hoffmann, J. Pallmann, J. Schaber, L. Borchardt, W. Nickel, I. Senkovska, S. Rico-Francés, J. Silvestre-Albero, S. Kaskel, E. Brunner, *Chem. Mater.* **2014**, *26*, 3280-3288.

[20] M. Oschatz, M. Leistner, W. Nickel, S. Kaskel, *Langmuir* **2015**, *31*, 4040-4047.

[21] M. Oschatz, M. Antonietti, *Energy Environ. Sci.* **2018**, *11*, 57-70.